Inversion of IceBridge gravity data for continental shelf bathymetry beneath the Larsen Ice Shelf, Antarctica

James R. COCHRAN, Robin E. BELL

Lamont–Doherty Earth Observatory, Columbia University, Palisades, NY, USA
E-mail: jrc@ldeo.columbia.edu

ABSTRACT. A possible cause for accelerated thinning and break-up of floating marine ice shelves is warming of the water in the cavity below the ice shelf. Accurate bathymetry beneath large ice shelves is crucial for developing models of the ocean circulation in the sub-ice cavities. A grid of free-air gravity data over the floating Larsen C ice shelf collected during the IceBridge 2009 Antarctic campaign was utilized to develop the first bathymetry model of the underlying continental shelf. Independent control on the continental shelf geologic structures from marine surveys was used to constrain the inversion. Depths on the continental shelf beneath the ice shelf estimated from the inversion generally range from about 350 to 650 m, but vary from <300 to >1000 m. Localized overdeepenings, 20–30 km long and 900–1000 m deep, are located in inlets just seaward of the grounding line. Submarine valleys extending seaward from the overdeepenings coalesce into two broad troughs that extend to the seaward limit of the ice shelf and appear to extend to the edge of the continental shelf. The troughs are generally at a depth of 550–700 m although the southernmost mapped trough deepens to over 1000 m near the edge of the ice shelf just south of 68° S. The combination of the newly determined bathymetry with published ice-draft determinations based on laser altimetry and radar data defines the geometry of the water-filled cavity. These newly imaged troughs provide a conduit for water to traverse the continental shelf and interact with the overlying Larsen C ice shelf and the grounding lines of the outlet glaciers.

1. INTRODUCTION

Warming in the region of the Antarctic Peninsula is one of the most prominent climate trends on the planet. Meteorological records since the middle of the 20th century show a temperature increase of $3.7 \pm 1.6^{\circ}\mathrm{C}\,(100\,\mathrm{a})^{-1}$ on the peninsula (Vaughan and others, 2003), several times greater than estimates of the global warming rate (e.g. Folland and others, 2001; Jones and Moberg, 2003; Smith and Reynolds, 2005; IPCC, 2007). Since Antarctica is the world's greatest reservoir of glacial ice, any changes in the volume of the Antarctic ice sheet resulting from warming can have a great effect on global sea level. Estimates of the potential rise in sea level resulting from melting of the West Antarctic ice sheet range from about 3.3 to 5.0 m (Mercer, 1978; Lythe and others, 2001; Bamber and others, 2009a).

Rignot and others (2008) used mass fluxes across glacier grounding lines determined from radar interferometry and snow accumulation from regional climate models to calculate the mass balance in the drainage basins of Antarctica. They found that most of East Antarctica has experienced a small 'near-zero' mass loss. On the other hand, major West Antarctic basins draining into the Amundsen Sea and drainage systems in the northern Antarctic Peninsula have experienced significant mass loss. These mass losses appear to have resulted from acceleration of the outlet glaciers and ice streams draining the basins, producing increased flux across the grounding line into the ocean.

Floating marine ice shelves can play an important role in moderating mass flux across the grounding line by serving as buttresses slowing the flow of inland ice into the sea. The presence of an ice shelf can provide a back-stress that inhibits ice-sheet advance behind the ice shelf (Dupont and Alley, 2005), thus limiting the flux of ice across the grounding line. Acceleration of glaciers following removal of the ice shelf was noted at Larsen A by Rott and others (2002) and De Angelis and Skvarca (2003) and at Larsen B by Rignot and others (2004). The role of the ice shelf is highlighted by the observation that while glaciers that were previously buttressed by the Larsen B ice shelf accelerated after the ice-shelf collapse, glaciers further south that feed into the remnant of the Larsen B ice shelf in SCAR Inlet did not accelerate (Rignot and others, 2004).

There is an ongoing discussion concerning the processes driving ice-shelf break-up involving the relative roles of surface processes such as the collection of surface melt in ponds and crevasses (e.g. Vaughan and Doake, 1996; Scambos and others, 2000, 2009; MacAyeal and others, 2003), stresses resulting from flow, rheology and the bounding geometry of the ice shelf (e.g. Doake and others, 1998; Vieli and others, 2006; Glasser and Scambos, 2008) and basal processes such as basal melting by warm water (e.g. Shepherd and others, 2003, 2004; Jenkins and others, 2010). In particular, although there is evidence that deep water in the Weddell Sea is warming (Robertson and others, 2002), there is uncertainty about whether this has contributed to accelerated melting of the Larsen Ice Shelf (Shepherd and others, 2003; Nicholls and others, 2004; Holland and others, 2009). Understanding water circulation beneath the large ice shelves is key to understanding the basal processes that may contribute to rapid break-up.

Modeling interactions between the ice shelf and water beneath it and understanding their impact requires knowledge of the geometry of the cavity. Knowledge of sub-ice geometry has come slowly, as it requires accurate measurements of the ice thickness and the underlying bathymetry. Radar can be used to determine the ice thickness and the upper surface of the cavity (e.g. Holland and others, 2009), but cannot penetrate the water underneath. Seismic techniques can be used to determine ice thickness and sea-floor depth beneath ice shelves, but is a time-consuming process.

https://doi.org/10.3189/2012JoG11J033 Published online by Cambridge University Press

For example, Johnson and Smith (1997) were able to obtain 152 spot measurements of ice thickness and sea-floor depth in the southern and western Ronne Ice Shelf during an entire field season. They merged their data with the compilation by Vaughan and others (1995) of previously existing data to produce a bathymetry map of the Filchner–Ronne Ice Shelf, which they estimate to have 10–100 km spatial resolution. There are presently only two published seismic spot measurements of the sea-floor depth beneath the Larsen C ice shelf (Jarvis and King, 1993, 1995). Exploration and mapping of bathymetry beneath floating ice with autonomous underwater vehicles (AUVs) has been undertaken at Pine Island Glacier (Jenkins and others, 2010), but is also a slow and difficult process.

The purpose of this paper is to use recently acquired Operation IceBridge (OIB) airborne gravity data to determine the bathymetry of the continental shelf beneath the Larsen C ice shelf. We have used the OIB airborne gravity data along with existing marine data to build a free-air anomaly map of the Larsen region. Using a standard inversion technique, we have developed the first robust model for the bathymetry beneath the Larsen C ice shelf. Marine gravity, bathymetry and seismic reflection data from the region just to the northeast enable us to isolate the signature of variations in geology from the bathymetry.

2. THE LARSEN ICE SHELF

The Larsen Ice Shelf extends along the eastern side of the Antarctic Peninsula from about 65°30′ S to 74°20′ S (Fig. 1). Prior to 1995, the ice shelf stretched northward to about 64°20′ N. The Larsen A ice shelf, the portion of the Larsen Ice Shelf north of Robertson Island and Seal Nunataks (~65° S), collapsed in January and February of 1995 (Rott and others, 1996; Skvarca and others, 1999). Larsen B, the portion of the ice shelf between Robertson Island and the Jason Peninsula (Fig. 1), began to retreat in 1995 and collapsed in 2002 (Scambos and others, 2003; Rack and Rott, 2004; Glasser and Scambos, 2008). The broad Larsen C ice shelf, which is the subject of this study, extends from the Jason Peninsula south to the Gibbs ice rise near 68°45′ S. The much narrower Larsen D ice shelf extends south from there to the Smith Peninsula at 74°20′ S.

The Larsen C ice shelf has an area of over 50 000 km^2. The ice shelf has been relatively stable over the time for which observations are available. Following a major calving event in 1986, it has slowly advanced and is at about 90% of its pre-calving size (Cook and Vaughan, 2010). The elevation of the ice surface is generally 40–60 m (Bamber and others, 2009b) and the thickness of the floating ice is 250–350 m (Griggs and Bamber, 2009; Holland and others, 2009) through much of the Larsen C area. Ice thickness varies along flowlines from >500 m at the grounding lines of major glaciers to about 250 m at the eastern edge. Shepherd and others (2003) used satellite altimeter data to show that the upper surface of the Larsen C ice shelf lowered at a mean rate of 0.08 ± 0.04 m a^{-1} in the period 1992–2001, reflecting thinning of the ice shelf. The rate of change of elevation increases from south to north, reaching 0.27 ± 0.11 m a^{-1}. Shepherd and others (2003) also used airborne radar measurements and the compilation of Lythe and others (2001) to determine that the Larsen C ice shelf has thinned at an average rate of 0.29 ± 0.68 m a^{-1} since 1966. They concluded that the thinning must result from a combination of increased summer melt and loss of basal ice through melting.

The only water-depth measurements beneath the Larsen C ice shelf are from two seismic experiments at 67°30′ S (locations shown on Fig. 2) (Jarvis and King, 1993, 1995). Jarvis and King (1993) obtained a depth to the sea-floor below the ice surface of 657 m at a 'walk-away' seismic experiment at 67°30′ S, 64°20′ W, while Jarvis and King (1995) obtained a depth to the sea-floor below the ice surface of 617 m at a reflection/refraction experiment centered at 67°30′ S, 63°43.5′ W. Using ice surface elevations from Bamber and others (2009b), these results give sea-floor depths of 602 and 563 m, respectively.

Bathymetry data from shipboard surveys are available for parts of the former Larsen A and Larsen B regions as well as the continental shelf to the east (e.g. Sloan and others, 1995; Pudsey and others, 2001, 2006; Smith and Anderson, 2010) (Fig. 3). The continental shelf is generally at a depth of 350–550 m and the shelf break, located near 54°30′ W, is very sharp and abrupt. A broad trough, reaching deeper than 500 m, cuts across the shelf perpendicular to the shelf break (Sloan and others, 1995; Pudsey and others, 2006). Narrow deep troughs reaching 900 m are located near the coast just seaward of substantial outlet glaciers (Pudsey and others, 2001) (Fig. 3). These troughs are about 20–30 km long and 10 km wide (Pudsey and others, 2006).

3. OPERATION ICEBRIDGE GRAVITY DATA

The Ice, Cloud and land Elevation Satellite (ICESat) was launched by NASA in 2003 to monitor ice-sheet mass balance using a laser altimeter. Its science mission ended in February 2010 following the failure of the last of its three lasers. A follow-on satellite, ICESat-2, is scheduled to be launched in the 2015–16 time frame. OIB was organized by NASA to continue to monitor the cryosphere during the hiatus between the two ICESat missions. OIB utilizes measurements from aircraft to maintain the altimetry time series and monitor important areas of land-based ice and sea ice. In addition to laser altimeters, OIB instrumentation includes a variety of ice-penetrating radars and a gravimeter. These tools expand the range of measurements to include the collection of data necessary to determine ice thickness and structure, bed topography underlying land-based ice, bathymetry beneath floating ice, snow accumulation and firn structure.

3.1. AIRGrav airborne gravity system

OIB gravity data were obtained with a Sander Geophysics AIRGrav airborne gravimeter. The AIRGrav system consists of a three-axis gyro-stabilized Schuler-tuned inertial platform on which three orthogonal accelerometers are mounted. The primary gravity sensor is the vertical accelerometer which is held within 10″ (0.0028°) of the local vertical by the inertial platform, monitored through the complex interaction of gyroscopes and two horizontal accelerometers (Sander and others, 2004). An advantage of the AIRGrav system over other airborne gravimeters is that it is capable of collecting high-quality data during draped flights (Studinger and others, 2008).

The gravimeter records accelerations arising both from variations in the Earth's gravity field and accelerations experienced by the airplane. These accelerations are recorded at 128 Hz. Aircraft accelerations are obtained utilizing differential GPS measurements. The gravimeter data

https://doi.org/10.3189/2012JoG11J033 Published online by Cambridge University Press

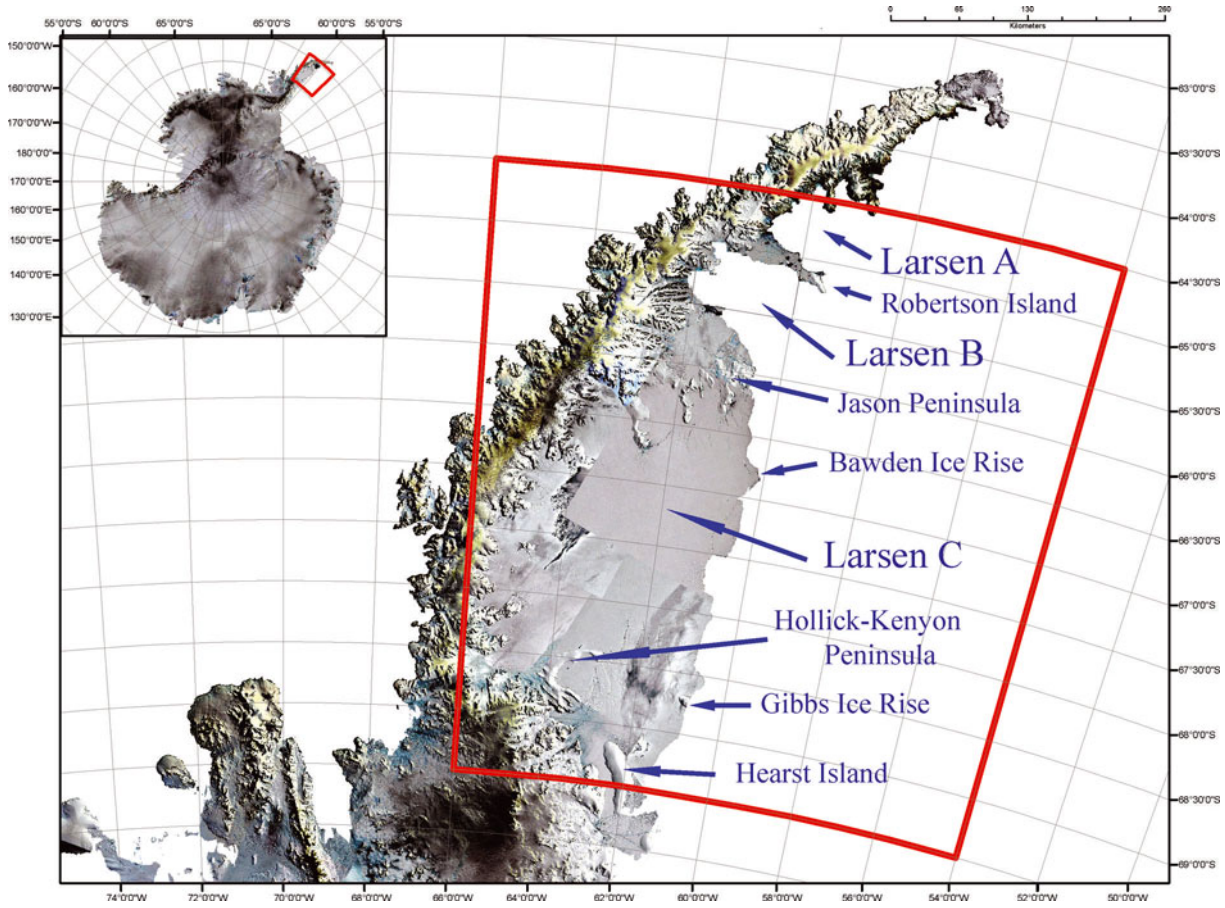

Fig. 1. Map of the Antarctic Peninsula showing the location of the Larsen C ice shelf, the former Larsen A and Larsen B ice shelves and other geographic features mentioned in the text. Red boxes show the region of the bathymetry maps shown in Figures 4 and 8. The images are a LIMA (Landsat Image Mosaic of Antarctica)/MODIS (Moderate Resolution Imaging Spectroradiometer)/RADARSAT mosaic of Antarctica from the Polar Geospatial Center at the University of Minnesota.

are filtered and decimated to 10 Hz to match the GPS data, and the GPS-derived aircraft accelerations are subtracted from the data. The gravity is corrected for the Eötvös effect, and the expected gravity at the measurement latitude is subtracted. The resulting anomalies are decimated to 2 Hz, low-pass filtered to suppress noise and the free-air correction is applied.

After evaluating the noise level with different filter lengths, we used a 70 s filter for the data presented in this study. The filter half-wavelength is ~5 km at the average flight speed of 275 kn (142 m s^{-1}) for our survey. Features narrower than the half-wavelength can be resolved, but will have an attenuated amplitude. Horizontal accelerations associated with turns and other vigorous maneuvers disturb gravity measurements. A routine that examines horizontal accelerations was used to divide each flight into lines that are free of these perturbations.

3.2. Free-air gravity anomalies

One of the critical areas targeted by OIB is coastal West Antarctica including the Antarctic Peninsula. Portions of three OIB flights were located over the Larsen C ice shelf during the 2009 campaign. These flights were flown at a height of ~1500 ft (457 m) above the ice surface at an average speed of ~275 kn (142 m s^{-1}). The average height above sea level was 515 m. The spacing of north–south airborne gravity lines is generally about 20 km, while the spacing of east–west lines ranges from 15 to 50 km (Fig. 2). The line spacing and the survey design limit the granularity of the gravity field and will impact the spatial resolution of our final bathymetry model.

We utilized the marine gravity and bathymetry data available in the region to augment the inversion of the airborne gravity. Bathymetry and gravity data collected aboard research ships are available for portions of the continental shelf adjacent to the Larsen Ice Shelf to the north of about 66°30′ S. Bathymetry contours determined from these data are shown in Figure 3. We gridded the marine free-air gravity data, upward-continued it to the elevation of the OIB flights over the Larsen C ice shelf and resampled the upward-continued grid at the original measurement locations. The combined dataset was gridded and contoured to produce the free-air anomaly map shown in Figure 2. Track lines are superimposed on the gravity map. Airborne gravity lines are in blue and ship tracks are in purple. The primary gaps in coverage are over the Jason Peninsula and to the east of Robertson Island.

Maximum free-air gravity anomalies of ~70 mGal are found at the continental shelf edge gravity high. The free-air gravity field away from the shelf edge has an average value of about 10 mGal. Isolated highs of >40 mGal are found at ~66°25′ S, 62°45′ W near the Churchill Peninsula and at the edge of the ice shelf near 66°50′ S, 60° W (Fig. 2). Gravity minima less than –30 mGal are situated near 68°15′ S, 61° W to the northeast of the Hollick–Kenyon Peninsula and just seaward of the grounding lines of major glaciers feeding

https://doi.org/10.3189/2012JoG11J033 Published online by Cambridge University Press

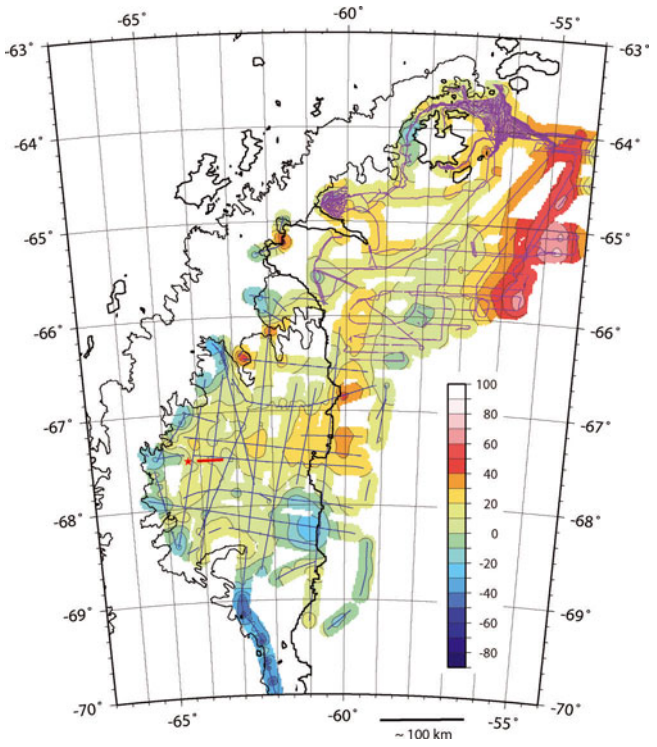

Fig. 2. Free-air gravity anomaly map of the Larsen Ice Shelf and adjoining continental shelf contoured at 10 mGal intervals. Map is based on IceBridge airborne gravity data and shipboard data upward-continued to the altitude of the flight-lines gridded at 2 km intervals. Areas >10 km from a data point are masked. The red star and line near 67°30′ S, 64° W show the location of British Antarctic Survey seismic experiments (Jarvis and King, 1993, 1995). Locations of airborne gravity measurements are shown in blue and locations of shipboard gravity measurements are shown in purple.

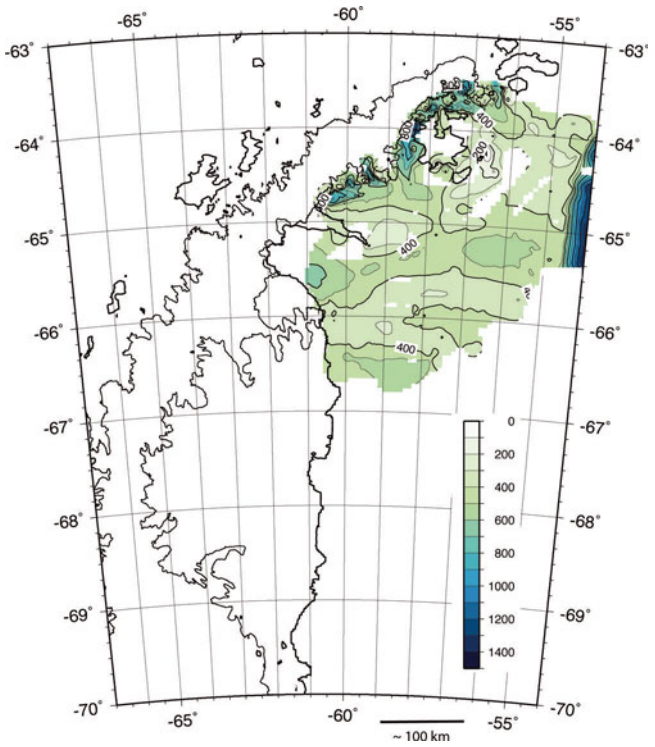

Fig. 3. Bathymetry of the continental shelf to the northeast of the Larsen Ice Shelf contoured at 100 m intervals based on available shipboard depth measurements. Areas >10 km from a data point are masked.

the Larsen Ice Shelf. The most negative gravity anomalies are found south of the Larsen C ice shelf on a flight-line along Stefansson Sound between Hearst Island and the mainland (Fig. 2).

4. INVERSION OF GRAVITY DATA FOR CONTINENTAL SHELF BATHYMETRY

We limit our analysis to the region seaward of the grounding line. By Archimedes' principle, floating ice displaces its weight in water and does not affect the total mass present. It can then be shown by the Bouguer gravity formula (Turcotte and Schubert, 2002, p. 210) that the presence of the floating ice does not affect the gravity anomalies measured above it, so we can ignore the ice in the inversion.

Inversion of the gravity data for bathymetric relief on the continental shelf was carried out using the Parker–Oldenburg technique (Oldenburg, 1974). Parker (1973) expressed the Fourier transform of the gravity anomaly resulting from relief on a horizontal interface in terms of powers of the Fourier transform of the topographic relief:

$$F[\Delta g(x\pm, y)] = -2\pi G\rho e^{-kz_0} \sum_{n=1}^{\infty} \frac{k^{n-1}}{n!} F[h^n(x, y)] \quad (1)$$

where F is the Fourier transform of the quantity in brackets, $\Delta g(x,y)$ is the gravity anomaly on the surface $z=0$, G is the gravitational constant, $h(x,y)$ is the depth to the interface (positive downward), ρ is the density contrast across the interface, k is the wavenumber and z_0 is the mean depth to the interface.

Oldenburg (1974) rearranged Parker's equation into an expression that allows computation of the depth to the undulating interface from the gravity anomaly through an iterative process:

$$F[h(x, y)] = -\frac{F[\Delta g(x, y)]e^{kz_0}}{2\pi G\rho} - \sum_{n=2}^{\infty} \frac{k^{n-1}}{n!} F[h^n(x, y)]. \quad (2)$$

We employed the Parker–Oldenburg inversion in the form of a MATLAB script developed by Gómez-Ortiz and Agarwal (2005) that utilizes a grid of gravity anomalies as the input. In order to avoid potential artifacts in less constrained areas, the grid of depths resulting from the inversion was sampled at gravity measurement points and these values were then regridded.

The term $F[\Delta g(x, y)]e^{kz_0}$ in Eqn (2) is numerically equivalent to downward continuation of the gravity data by a distance z_0. Since downward continuation amplifies high-frequency noise in the data, it is necessary to ow-pass filter the data to obtain a stable solution. We utilized a filter that passes full wavelengths of >25 km and rolls off at shorter wavelengths. This limits our ability to resolve narrow features.

4.1. Constraints on the Larsen inversion

Inversion of gravity anomalies for bathymetry assumes that the anomalies arise from bathymetric relief. There are two features in the Larsen region free-air gravity anomaly map (Fig. 2) that are not related to bathymetry. These features limit the area over which we can invert the gravity data for bathymetry, but also provide important clues on the appropriate density contrast to use for the inversion. The

https://doi.org/10.3189/2012JoG11J033 Published online by Cambridge University Press

gravity high extending north-northeast between 56° W and 54° W along the edge of the continental shelf is the most prominent gravity feature of the survey area. Shelf-edge gravity highs are a ubiquitous feature of continental margins and are part of an isostatic edge-effect anomaly resulting from the change in crustal thickness across the continental margin (e.g. Bell and others, 1990; Wyer and Watts, 2006).

The second gravity anomaly not present in the bathymetry is a gravity high that extends north–south along the edge of the ice shelf at 60° W from about 67°45′ S to 66° S where the trend changes to north-northeast–south-southwest and the anomaly becomes less distinct east of Robertson Island (Fig. 2). Marine seismic reflection studies show that this gravity high corresponds to a subsurface region of incoherent hyperbolic reflections typical of crystalline rock, which Sloan and others (1995) and Smith and Anderson (2010) interpret as Jurassic and younger volcanics. This unit deepens to the east and is onlapped by a sequence of continental shelf sediments extending eastward to the edge of the continental shelf, which Smith and Anderson (2010) argue were deposited during the period from the late Eocene to the present.

In light of these geologic complications, we limit the inversion to the area west of the 60° W basement ridge. Although the marine seismic reflection studies did not image the strata in this region, the gravity anomalies imply that their density must be slightly less than that of the buried crystalline basement ridge. Some evidence of their nature comes from seismic experiments carried out on the Larsen Ice Shelf at 67°30′ S by the British Antarctic Survey (BAS) and reported by Jarvis and King (1993, 1995) (Fig. 2). Jarvis and King (1993) found that the seabed has a very high reflection coefficient that they interpreted as showing the presence of crystalline rock with little or no sedimentary cover. In a reflection/refraction experiment centered about 30 km to the east, Jarvis and King (1995) found that the subsea bed lacked internal reflectors. This is a different response from the strong reflectors from a stratified sedimentary sequence that they observed under the Ronne Ice Shelf using similar techniques. Jarvis and King (1995) concluded that significant quantities of sedimentary material are absent from their Larsen survey area.

Jarvis and King (1995) were unable to determine the velocity immediately below the sea-floor because the water acts as a low-velocity layer. They assumed the presence of an upper layer (unit 1) with a seismic velocity of 2.8 km s^{-1} in their interpretation. The velocities of the deeper layers (units 2 and 3) are well defined by expanding spread data.

We will assume that the gravity anomalies arise primarily from relief on the top surface of their unit 2, which has a seismic P-wave velocity of 4.7 km s^{-1}. Unit 2 contains few internal reflectors and is not a stratified sediment sequence such as observed on the outer Larsen continental shelf. Jarvis and King (1995) interpreted unit 2 as Cretaceous calc-alkaline lavas of the Antarctic Peninsula volcanic group. We assume a density of 2.70 g cm^{-3} (density contrast of 1.67 g cm^{-3}) for the inversion. This is consistent with density measurements on Antarctic Peninsula Volcanic Group rocks reported by Renner and others (1985) and with empirical velocity–density relationships (e.g. Ludwig and others, 1971; Carlson and Raskin, 1984).

We thus assume that the sea-floor beneath the Larsen C ice shelf consists of these volcanic sequences with only a thin or discontinuous layer of low-density sediments, as observed by Jarvis and King (1993, 1995) in their study area. A number of regional studies have assumed that a thick sequence of Upper Cretaceous sediments observed on James Ross Island extends southward for several hundred kilometers beneath the ice shelf to form a Larsen sedimentary basin (e.g. Macdonald and others, 1988; Del Valle and others, 1992; Hathway and others, 1998; Hathway, 2000). The presence of this basin was inferred primarily on the basis of an abrupt change from high-amplitude short-wavelength aeromagnetic anomalies over the mainland to low-amplitude long-wavelength anomalies over the Larsen Ice Shelf (Renner and others, 1985; Macdonald and others, 1988; Maslanyi and others, 1991) and an outcrop of similarly aged sediments on Table Nunatak, at the tip of the Kenyon Plateau (Hathway and others, 1998). The seismic experiments of Jarvis and King (1993, 1995) were conducted within the area of low magnetic gradients with the goal of characterizing the Larsen basin sediments believed to lie below. They did not find the expected sedimentary sequence and concluded that, if the basin exists, it must be located farther to the east. We see no evidence, either in gravity anomalies (Fig. 2) or in aeromagnetic anomalies (Renner and others, 1985; Maslanyi and others, 1991), for the presence of a large north–south trending sedimentary basin between the Jarvis and King (1993, 1995) seismic experiments and the 60° W gravity high.

The free parameters in the inversion are the density contrast across the interface and the average depth of the interface below the measurement level. We assume a density contrast of 1.67 g cm^{-3}. Based on the geologic framework outlined above, we believe that the uncertainty in the density contrast is $<\pm 0.1$ g cm^{-3}. We also assume a distance of 1.05 km below the average flight depth (535 m below sea level) as the average depth of the continental shelf. We believe that the density contrast is better constrained than the average depth, so we did inversions for our preferred density contrast for a range of average depth below the flight-lines (900–1200 m, implying average continental shelf depths of 385–685 m below sea level). We selected the average depth that provided the best match in our results to observed depths in the two widely separated areas, the former Larsen B and the Jarvis and King seismic lines, which provide control. The effects of uncertainties in density contrast and average depth are discussed below in Section 4.3.

4.2. Larsen shelf bathymetry

The results of our inversion of the gravity data for bathymetric relief beneath the Larsen C ice shelf are shown in Figure 4 along with the shipboard bathymetry to the north and east of the airborne survey. Areas >10 km from a data point have been masked. We also show flight-lines (in blue) and ship tracks (in purple). The depth of the continental shelf beneath the Larsen Ice Shelf is generally in the range ~350–650 m, but ranges from <300 to >1000 m. The main features are a series of overdeepenings reaching 1000 m along the grounding lines of major glaciers feeding the ice shelf and three broad troughs across the shelf.

There are two areas where the results of the inversion can be tested against known bathymetric depths. One is at the location of the seismic experiments of Jarvis and King (1993, 1995) (Fig. 5). Jarvis and King (1993) determined a depth from the top of the ice to the sea-floor of 657 m at 67°30′ S, 64°20′ W from their 'walk-away' seismic experiment. Using an ice surface elevation of 55 m from the Bamber and others

https://doi.org/10.3189/2012JoG11J033 Published online by Cambridge University Press

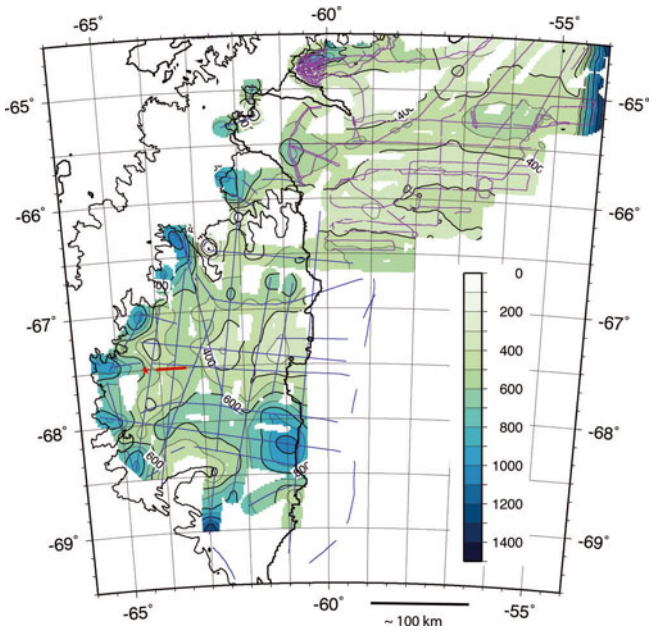

Fig. 4. Bathymetry beneath the Larsen Ice Shelf determined from inversion of airborne gravity data and on the adjacent continental shelf from shipboard measurements contoured at 100 m intervals. Areas >10 km from an airborne gravity or marine bathymetry measurement are masked. The red star and line near 67°30′ S, 64° W show the location of BAS seismic experiments (Jarvis and King, 1993, 1995). Locations of airborne gravity measurements are shown in blue and locations of shipboard bathymetry measurements are shown in purple.

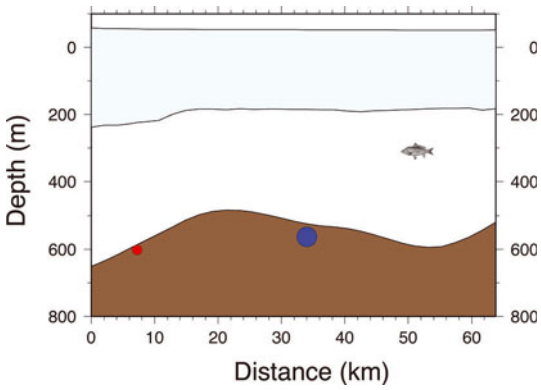

Fig. 5. West to east profile across the Larsen Ice Shelf along 67°30′ S from 64°30′ W to 63° W. The sea-floor is shown in brown and the ice shelf in light blue. Sea-floor is from our inversion. The top of ice is from the Bamber and others (2009a) DEM and base of ice is determined from ice-thickness values in Holland and others (2009). The red circle shows the sea-floor depth determined from the 'walk-away' seismic experiment of Jarvis and King (1993) at 67°30′ S, 64°20′ W. The blue circle shows the sea-floor depth determined from the seismic refraction experiment of Jarvis and King (1995) extending from 67°30′ S, 64°05′ W to 67°30′ S, 63°22′ W. The circle is at the midpoint of the seismic line. The diameters of the circles are scaled to the estimated uncertainty in the seismically determined depths.

(2009b,c) Antarctic digital elevation model (DEM), this gives a water depth of 602 m which is 16 m deeper than the sea-floor depth of 586 m predicted by our inversion at that location. Sampling our bathymetry grid along the Jarvis and King (1995) refraction line shows a variation in depth from 500 to 582 m, with a mean depth of 539 m. Jarvis and King (1995) report an ice-surface to sea-floor distance of 617 m. Using an ice surface elevation of 54 m from Bamber and others (2009b,c) gives a depth below sea level to the sea-floor of 563 m, 24 m deeper than predicted by our inversion.

The second region where a comparison between observed and predicted depths is possible is the area of the former Larsen B ice shelf to the west of the buried crystalline ridge in the area where we believe the inversion to be valid. Over much of that area, the predicted depths are between 20 m shallower and 30 m deeper than the shipboard data (Fig. 6). However, in the center of Robertson Trough (Sloan and others, 1995; Evans and others, 2005), the predicted depths rapidly increase to 100–120 m deeper than the shipboard data. This appears to be the result of low-density sediments underlying the deepest portion of the trough. A simple gravity model shows that, if the average sediment density is 2.2 g cm^{-3}, then about 500 m of sediment is necessary to explain the difference between the observed and modeled depths. The shipboard bathymetry lines across Robertson Trough are through the deepest portion of the trough (Fig. 3). The mismatch between the modeled and observed depths decreases markedly to the east as the trough shallows (Fig. 5c). It is possible that the sediments have accumulated in a locally deep portion of the trough.

If similar sediments underlie the two troughs to the south under the Larsen C ice shelf, we may also have overestimated their depths by as much as 120 m in portions or perhaps much of those troughs. Away from the center of Robertson Trough, the results of the inversion in Larsen B consistently agree with the available shipboard depth measurements to within ±35 m and we have no reason to assume that is not the case in the ice-covered region of the Larsen C ice shelf. That conclusion is consistent with the depths recorded at the Jarvis and King (1993, 1995) seismic sites.

4.3. Uncertainties in the inversion

As discussed above, the free parameters in the inversion are the average depth and the bed density. We tested the sensitivity of the solution to variations in these parameters by repeating the inversion with different values. Figure 7 shows the depth differences when a density of 2.6 g cm^{-3} rather than 2.7 g cm^{-3} is assumed. In Figure 7, positive values mean that the bathymetry using a density of 2.6 g cm^{-3} is shallower and negative values mean that the area is deeper. The shape of the contours in the difference map (Fig. 7) is very similar to those on the depth map (Fig. 4). This is because, with the reduced density contrast, areas shallower than the mean depth need additional mass to match the observed gravity, while areas deeper than the mean depth need a greater mass deficiency. Thus shallow areas become shallower, and deep areas become deeper. If we had increased rather than decreased the density, the opposite would have occurred. The largest depth changes are about ±30–35 m. The largest changes are confined to the very deepest and very shallowest regions. Throughout most of the area, which is within a few hundred meters of the mean depth, depth changes due to a 0.1 g cm^{-3} variation in density are <10–15 m. We ran inversions for an array of density contrasts and found that, within the range of plausible seabed densities (~2.45–2.90 g cm^{-3}), the inferred depth at a particular location varies nearly linearly with the density contrast. The sign of the variation depends on whether the location is

https://doi.org/10.3189/2012JoG11J033 Published online by Cambridge University Press

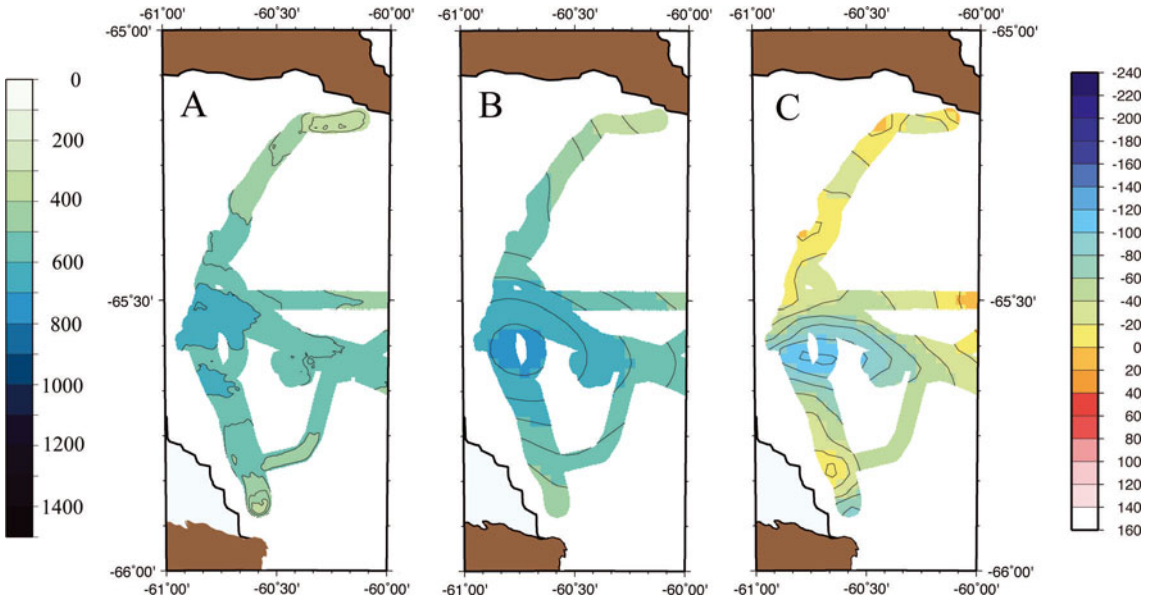

Fig. 6. Comparison of depths determined from our inversion and shipboard data in the area of the former Larsen B ice shelf. Map A shows the shipboard swath bathymetry gridded on a 200 m grid. Map B shows our inversion of the IceBridge airborne and upward-continued shipboard gravity data in the same region on a 2 km grid. Contours are at 50 m intervals, and color changes at 100 m intervals, on both maps. Map C shows the difference between the shipboard and predicted depths on a 2 km grid. Positive differences are where the predicted depths are shallower, and negative differences where they are deeper than the shipboard measurements. Color changes and contours are at 20 m intervals. Differences are generally between +20 and –30 m except near the deepest part of Robertson Trough, where the difference increases rapidly to >100 m.

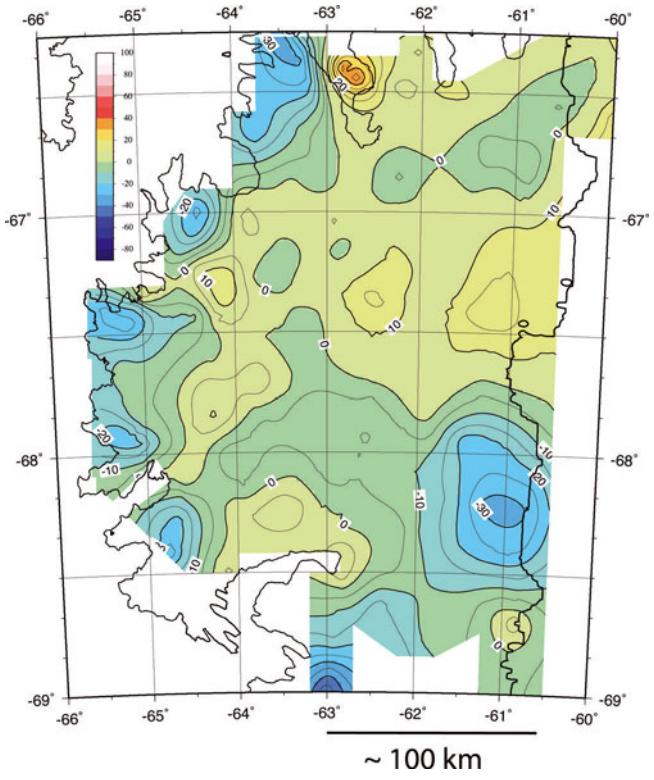

Fig. 7. Changes in the calculated bathymetry beneath the Larsen C ice shelf resulting from a change in the assumed bed density from 2.70 to 2.60 g cm^{-3}. Contour interval is 5 m and color changes are at 10 m intervals. Sign convention is that positive areas have become shallower and negative areas have become deeper. Maximum changes are about ±35 m.

above or below the mean depth, and the scale factor varies with the relative distance from the mean depth.

We also investigated the effect of changing the mean depth, which is the other free parameter, by repeating the original inversion assuming a mean depth of 425 m (975 m below the average flight height), 75 m less than in the original inversion. This basically resulted in a DC shift of 75 m in the derived depths. Depths at all points were shallower by 69–80 m than in the original inversion, with shallow areas at the low end and deeper areas at the higher end of that range.

The possible presence of low-density sediments also adds uncertainty to the inversion. The presence of sediments in the three major troughs may cause us to overestimate their depths by as much as 120 m. The available data suggest that significant sediment deposits are limited to the deeper portions of the three major troughs. The Jarvis and King (1995) seismic reflection line runs down one side and across the bottom of a north–south trending bathymetric depression (Fig. 4) at a depth of just under 600 m. No sediment cover was resolved on the profile. Jarvis and King (1993) found that the seabed has a high reflection coefficient and a high refraction velocity and interpreted it as consisting of crystalline rock. They state 'there is little or no sedimentary cover in the survey area' (Jarvis and King, 1993, p. 77). Jarvis and King (1995) also report a high refraction velocity as well as a lack of coherent sub-bottom reflectors in their refraction/reflection line. They conclude that there is not a sedimentary sequence present in their survey area, but rather, at most, a thin veneer of till. The presence of crystalline rock at the sea-floor is consistent with observations made at many formerly ice-covered portions of the continental shelf of West Antarctica, where exposed crystalline bedrock is commonly found on the inner half of the continental shelf (Wellner and others, 2001).

https://doi.org/10.3189/2012JoG11J033 Published online by Cambridge University Press

5. DISCUSSION

5.1. Shelf transverse troughs

The main features of the Larsen C continental shelf bathymetry are a series of overdeepened depressions or marginal troughs near the grounding line, and two broad transverse troughs extending across the shelf (Fig. 8). A similar pattern of morphology is observed in the shipboard bathymetric data in the Larsen A and B areas.

Overdeepened marginal troughs under Larsen C are located at ~50 km intervals along the grounding line, proximal to the mouths of inlets that are fed by several glaciers. Specifically they are centered near 68°25′ S (Mobil Oil Inlet), 67°54′ S (Seligman Inlet), 67°26′ S (Whirlwind Inlet), 67° S (Mill Inlet) and 66°20′ S (inner portion of Cabinet Inlet). The gravity data also reveal an overdeepened trough at 65°48′ S near the grounding lines of Leppard and Flask Glaciers at the western edge of SCAR Inlet in Larsen B.

The grounding-line troughs identified from the gravity inversion are about 20 km long by 12 km wide, with depths of 900–1050 m. These dimensions are similar to a trough in the Larsen A area just seaward of the grounding line of Drygalski Glacier (64°45′ S, 60°20′ W) observed in the shipboard bathymetric data (Del Valle and others, 1998; Pudsey and others, 2001) (Figs 4 and 8). Because of the low-pass filtering necessary for the inversion, the troughs may actually be slightly deeper and narrower.

Channels extending seaward from the grounding-line overdeepenings coalesce to form broad troughs that continue across the shelf to the seaward edge of our data. The northern trough, which was recognized in shipboard bathymetry data and given the name Robertson Trough by Sloan and others (1995), can be traced to the edge of the continental shelf. There are no shipboard bathymetry data available south of about 66°30′ S (Fig. 3). Bathymetry derived from satellite altimetry (Smith and Sandwell, 1997) shows a feature that appears to be a seaward extension of the central (Jason) trough to the edge of the continental shelf. The quality of the satellite-derived bathymetry deteriorates rapidly south of 67°30′ S due to increased sea-ice cover, making it impossible to determine if the southern (Kenyon) trough extends to the shelf edge. Since the two northern troughs reach the shelf edge, it is likely that Kenyon Trough also extends to the continental margin.

As first noted by Shepard (1931), broad troughs extending across the continental shelf are a common feature of glaciated and formerly glaciated continental margins in both the Northern Hemisphere and the Antarctic (e.g. Wellner and others, 2001; Nielsen and others, 2005). These troughs are characteristically 30–100 km wide with an undulating along-axis depth profile and can extend for several hundred kilometers. They are typically a few hundred meters deeper than the surrounding continental shelf, but can be as deep as 1000 m (Nielsen and others, 2005). The troughs are believed to have been formed by fast-flowing ice streams within the ice sheet that previously occupied the continental shelf. Jason Trough is 50–60 km wide and has an average depth of 550–600 m. This is about 250–300 m deeper than the central Larsen continental shelf to the south. The Jason Peninsula, which is above sea level, lies to the north (Fig. 8). Kenyon Trough to the west of 62° W is at a depth of ~650 m and is 40–60 km wide. Further east, near the edge of the ice shelf, it deepens to almost 1000 m and broadens out to be about 90 km wide. The dimensions

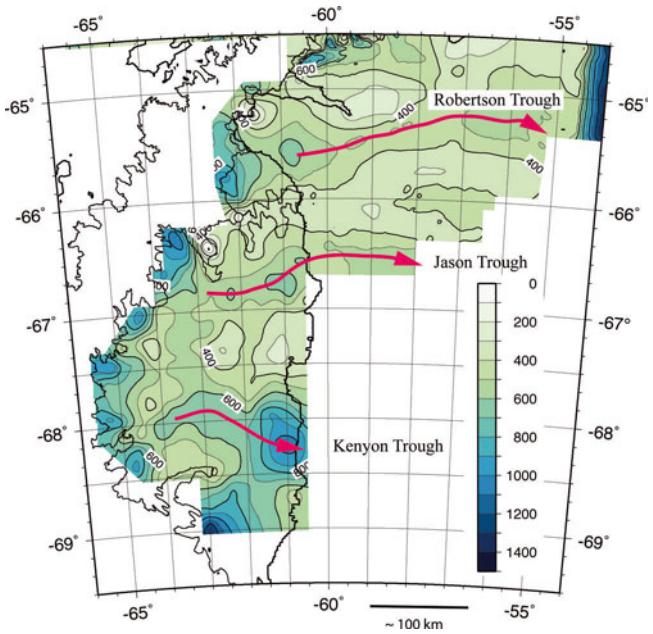

Fig. 8. Bathymetry beneath the Larsen Ice Shelf determined from inversion of airborne gravity data and, on the adjacent continental shelf, from shipboard measurements contoured at 100 m intervals. Red arrows show the location of broad glacial troughs across the continental shelf.

of the troughs across the continental shelf beneath the Larsen Ice Shelf are thus well within the globally observed range for glacial troughs.

5.2. Water-filled cavity below the Larsen Ice Shelf

Holland and others (2009) utilized radar data collected during 1997–98 along with BEDMAP ice thicknesses (Lythe and others, 2001) to map ice draft in the Larsen C area. We combined our seabed depths from the gravity inversion with Holland's ice-draft data to determine the size and geometry of the sea-water cavity (Fig. 9). Three east–west profiles of bathymetry, base of ice and top of ice are shown in Figure 10a. Profiles A and C follow the axes of Jason and Kenyon Troughs, respectively, and profile B is across the region of shallower bathymetry between the two troughs. Two north–south profiles are shown in Figure 10b. Profile locations are shown in Figure 10c.

The broad bank of relatively shallow bathymetry extending across the continental shelf at about 67° S to 67°40′ S effectively divides the cavity into two chambers centered on the troughs. Over much of the bank, the water layer under the ice is <150 m thick and in places is <50 m thick. Above the troughs, the water layer thickness is generally 350–450 m, but increases dramatically to 850 m to the east of 61° E in Kenyon Trough (Fig. 9).

A channel located near 63°15′ W provides a north–south connection between the two chambers. The thickness of the water layer in the channel is 250–350 m (Fig. 9) and the sea-floor is at a depth of 500–600 m. This channel is 100–200 m deeper than most of the rest of the bank between Jason and Kenyon Troughs (Fig. 10a, profile B) and is ~50–100 m shallower than in the troughs. Thus this channel could form part of a coherent water circulation system beneath the ice. There is also a north–south band of deeper sea-floor and a thicker water cavity just seaward of the grounding line. However, it is unclear from our gravity-based bathymetry

https://doi.org/10.3189/2012JoG11J033 Published online by Cambridge University Press

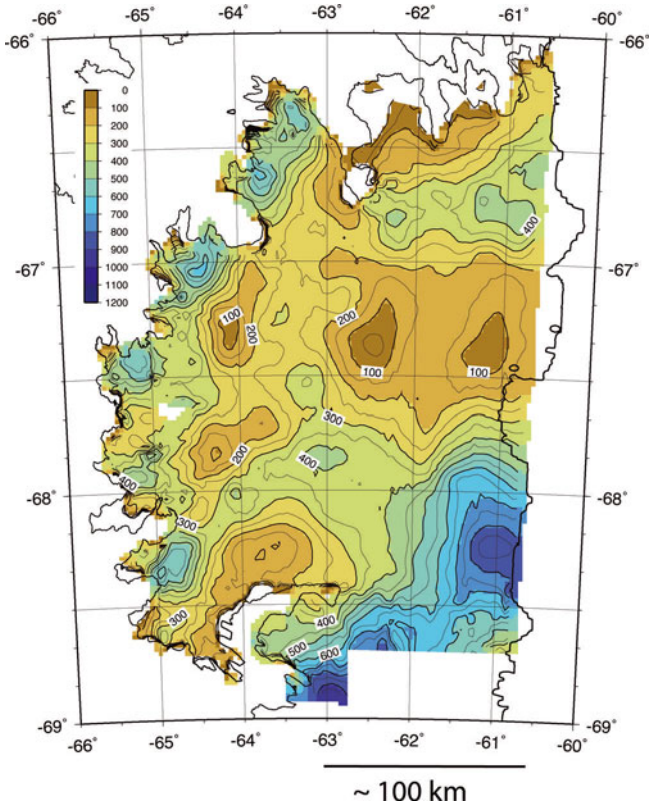

Fig. 9. Thickness of the water cavity beneath the Larsen Ice Shelf contoured at 50 m intervals. The cavity thickness is the difference between the sea-floor depth determined from our inversion and the ice draft determined by Holland and others (2009).

whether the grounding-line channel forms a continuous connection along the landward edge of the Larsen Ice Shelf.

5.3. The 60°E gravity high and stability of the ice front

Bathymetric sills can pin ice shelves and have the potential to serve as stabilizing points. The 60° E gravity high results from a subsurface volcanic ridge that has no sea-floor topographic expression through most of the area of marine surveys in the former Larsen B region (Sloan and others, 1995). South of about 66°15′ S, the gravity high begins to have a bathymetric expression and it may serve as a stabilizing sill. This can be seen in Figure 10a, profile A, where the bathymetric high centered at km 190 lies directly under the gravity high. Further south, Bawden Ice Rise, centered at 66°52′ S, 60°18′ W, is coincident with the maximum gravity anomaly along the 60° W gravity high (Fig. 2). Bawden Ice Rise is a 15 km × 4 km ice rise that Jansen and others (2010) describe as the easternmost pinning point of the Larsen B ice shelf. Interaction between Bawden Ice Rise and the ice shelf has generated a distinctive band of crevasses on the ice shelf (Glasser and others, 2009; Jansen and others, 2010).

Bawden Ice Rise clearly forms at a peak on the basement ridge. However, the gravity anomaly high continues south along the ice front with a significant amplitude to 67°40′ S (Fig. 2). Since the cavity between the ice and the sea-floor immediately to the west of the gravity high in this region is only 100–150 m (Fig. 9), any ridge associated with the gravity high would be very close to the base of the ice. Although direct interactions between the ice shelf and the sea-floor are only documented at Bawden Ice Rise, it is possible that the 60° W ridge has at times been in contact with the ice shelf and perhaps served to define and stabilize the ice front. Deflection of Jason and Kenyon Troughs around the region where the gravity high is best developed suggests interaction between the ice sheet that formerly covered the continental shelf and a basement ridge.

6. IMPLICATIONS

6.1. Circulation of sea water beneath the Larsen C ice shelf

Thinning and erosion of major ice shelves has been linked to the presence of relatively warm water at their base (Shepherd and others, 2003). Troughs cutting across the continental shelf, such as we have identified at the Larsen Ice Shelf, can provide a pathway for relatively warm water from ocean basins to reach floating ice shelves. In the Amundsen Sea, a number of oceanographic studies have shown the presence of almost undiluted Circumpolar Deep Water (CDW) >3°C above the in situ freezing point at the ice front of Pine Island Glacier (Jacobs and others, 1996; Jenkins and others, 1997; Hellmer and others, 1998). Jenkins and others (1997) estimate that two-thirds of the thinning (~360 m) over the final 70 km of Pine Island Glacier is due to melting from below. Walker and others (2007) investigated the oceanography of a trough, about 650 m deep and 50 km wide, leading from the Amundsen Sea shelf break at 114° W to Pine Island Bay (Dowdeswell and others, 2006). They found that the trough is filled with CDW and that the upper limit of CDW roughly corresponds to the depth of the outer continental shelf, so that the trough forms a pathway for the warm CDW to reach the ice front in Pine Island Bay.

The circulation and water masses in the Weddell Sea are significantly different from those in the Amundsen Sea. Also, there has not been a comprehensive oceanographic study of any of the Larsen Ice Shelf troughs such as carried out for the Amundsen Sea trough by Walker and others (2007). Warm Deep Water, also called Weddell Deep Water (WDW), is the primary warm water mass in the Weddell Sea. The upper boundary of WDW is usually defined as the 0.0°C isotherm, and its lower boundary is gradational with the underlying Weddell Sea Deep Water (WSDW) (e.g. Carmack and Foster, 1977; Meredith and others, 2000; Robertson and others, 2002). It has a salinity generally in the range 34.60–34.68 (e.g. Gordon and Huber, 1990; Weppernig and others, 1996; Robertson and others, 2002). WDW is found immediately below the pycnocline with its core at depths of 200–500 m in the middle of the gyre, well away from the continental margin (e.g. Gordon and Huber, 1995; Robertson and others, 2002).

There have been two major studies of the circulation and stratification in the western Weddell Sea. In 1992, the Ice Station Weddell program collected data from a floating ice camp along a profile extending from 71°48′ S to 65°38′ S roughly along 53°30′ W at about the 3000 m contour, 280 km east of the Larsen Ice Shelf (e.g. Gordon and ISW Group, 1993; Robertson and others, 1995; Gordon, 1998). The ice station measurements were supplemented by four helicopter-based profiles up to the continental shelf at 71° S, 68°40′ S, 67°40′ S and 65°50′ S. The Ice Station POLarstern (ISPOL) program in 2004 collected data on the water column from about 68.3° S to 66.9° S at 55.4° W in 1500 m of water, ~200 km east of the Larsen Ice Shelf (Absy and others, 2008).

https://doi.org/10.3189/2012JoG11J033 Published online by Cambridge University Press

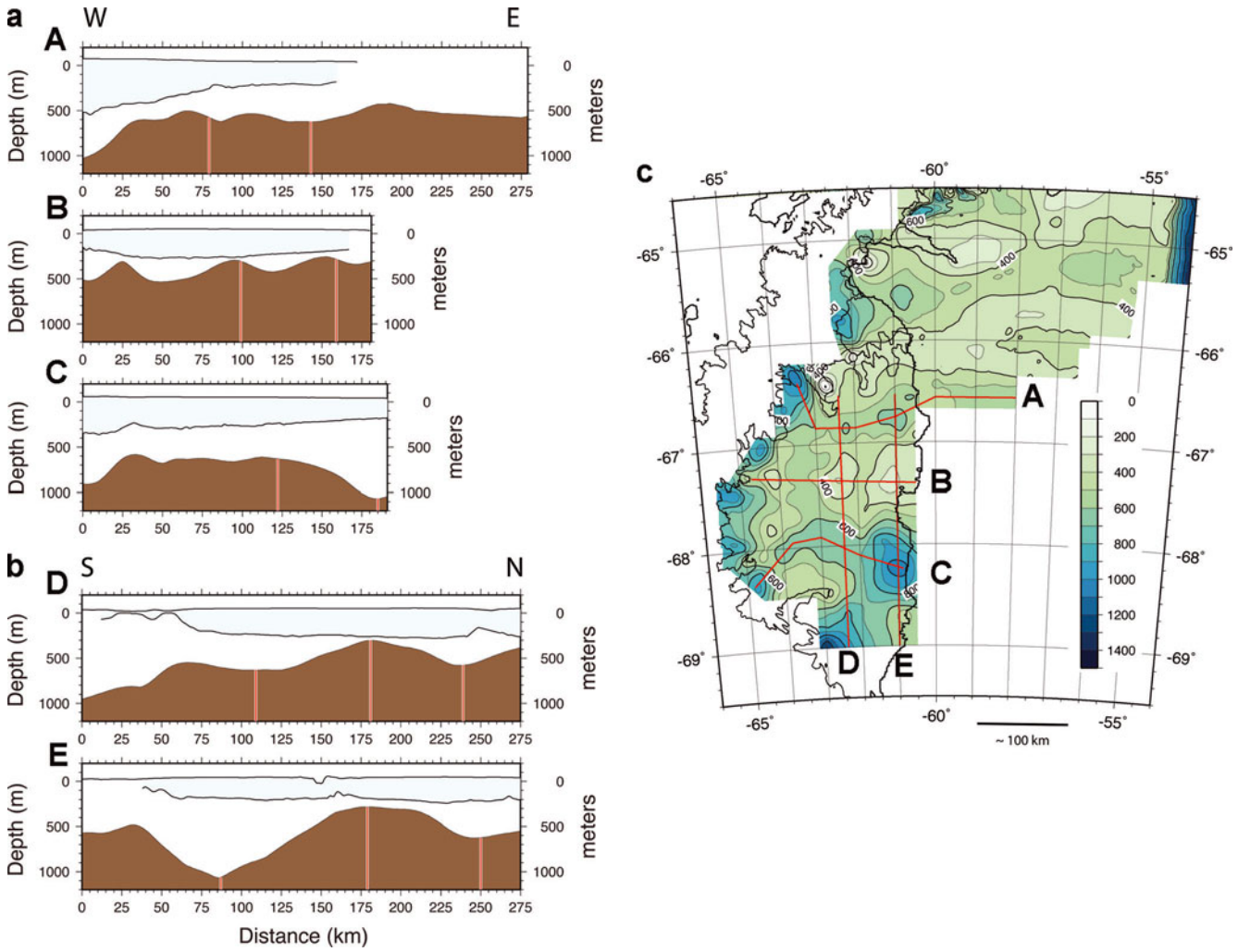

Fig. 10. (a) West–east profiles across the Larsen Ice Shelf showing the sea-floor (brown) and the ice shelf (light blue). Sea-floor is from our inversion and shipboard data. The top of ice is from the DEM of Bamber and others (2009b), and the base of the ice is from Holland and others (2009). Profiles A and C are along Jason and Kenyon Troughs, respectively, and profile B is across the shallow bank between the troughs. Red bars show crossings with profiles D and E shown in (b). Locations of profiles are shown in (c). West is to the left. Where the base of the ice does not extend as far as the upper surface, it is because the ice shelf extends beyond the grid of Holland and others (2009). (b) South–north profiles along the Larsen Ice Shelf showing the sea-floor (brown) and the ice shelf (light blue). Sea-floor is from our inversion, the top of the ice is from the DEM of Bamber and others (2009b) and the base of the ice is from Holland and others (2009). Red bars show crossings with profiles A–C shown in (a). Locations of profiles are shown in (c). South is to the left. Where the base of the ice does not extend as far as the upper surface, it is because the ice shelf extends beyond the grid of Holland and others (2009). (c) Bathymetry map of the region of the Larsen Ice Shelf showing the locations of the profiles shown in (a) and (b).

ISPOL also occupied stations reached by helicopter that form a profile to the edge of the continental shelf near 67°30′ S. These studies found that in the western Weddell Sea, approaching the continental margin, WDW becomes cooler and less salty and deepens to 500–800 m depth (e.g. Weppernig and others, 1996; Gordon, 1998; Robertson and others, 2002; Absy and others, 2008). This water is referred to as Modified Warm Deep Water (MWDW).

MWDW impinges on the continental margin below the general shelf level, but above the depth of the base of the troughs. Nicholls and others (2004) found MWDW at two stations in Jason Trough just to the east of the Larsen Ice Shelf. At stations in shallower water immediately to the east of the Jason Peninsula, they found much colder ice-shelf water (ISW), formed by the interaction of water with the base of the ice shelf. ISW has potential temperatures below the surface freezing point. This could be taken as evidence that MWDW is obtaining access to the base of the ice shelf through the troughs and is melting ice from the base of the ice shelf, so that warming of WDW (Robertson and others, 2002) could lead to an acceleration in the thinning of the ice shelf.

However, Nicholls and others (2004) argue that the salinity–temperature relationships that they observed in Larsen ISW imply that the ISW was not derived directly from MWDW but rather from MWDW that was preconditioned by winter cooling and sea-ice production. While they argue that this will insulate the ice shelf from possible warming of WDW, the data reported by Nicholls and others (2004) come from a few stations in a limited area and, in particular, their observations of ISW were made directly east of the Jason Peninsula rather than east of the Larsen C ice shelf. Further detailed oceanographic studies along the ice shelf are needed to document both the presence of MWDW in the troughs and the nature of the ISW resulting from interactions of the ice shelf with the underlying water.

https://doi.org/10.3189/2012JoG11J033 Published online by Cambridge University Press

7. SUMMARY AND CONCLUSIONS

1. A grid of airborne gravity data was collected over the Larsen C ice shelf during the 2009 OIB Antarctic campaign utilizing a Sander AIRGrav system mounted in a DC-8 aircraft and flown at an altitude of ~1500 ft (457 m) above the ice surface. The airborne data are supplemented by marine bathymetry, gravity and seismic reflection data in the region of the former Larsen A and B ice shelves and the continental shelf north of 66°30′ S. The gravity data were inverted to obtain bathymetric relief on the continental shelf beneath the ice shelf using the Parker–Oldenburg technique (Oldenburg, 1974). The shipboard data allowed us to isolate gravity anomalies arising from subsurface geology and structure from those arising from bathymetric relief. The inversion was limited to the region west of a buried volcanic ridge extending north–south near 60° W along the edge of the ice shelf. The bathymetry obtained from the inversion merges well with the shipboard bathymetry measurements from the region immediately to the north and east. Depths obtained from the inversion agree with the limited amount of available water-depth information from that area to ±35 m, although we may overestimate the depths at the bottom of the troughs extending across the continental shelf by as much as 100 m due to the presence of low-density sediments.
2. Depths on the continental shelf beneath the ice shelf determined from the inversion generally range from about 350 to 650 m, but vary greatly from <300 m to >1000 m (Fig. 4). Distinctive localized overdeepenings, 20–30 km long and 10–15 km wide and reaching 900–1000 m deep, are located near the grounding line in inlets where multiple glaciers converge. Submarine valleys extending seaward from the overdeepened areas coalesce into broad troughs that extend to the seaward limit of the ice shelf and appear to extend to the edge of the continental shelf. The troughs generally are at a depth of 550–700 m although the southernmost mapped trough (Kenyon Trough) deepens to >1000 m near the edge of the ice shelf just south of 68° S. Jason and Kenyon Troughs are separated by a shallow bank with minimum depths of ~275 m. The Jason Peninsula lies between Robertson and Jason Troughs. Seaward of the Jason Peninsula, the bank between those two troughs is at depths of 300–400 m (Figs 8 and 10). The shallow banks between the troughs divide the cavity beneath the ice shelf into chambers centered over the troughs. The water layer between these chambers is generally only 50–150 m thick, although north–south channels near 63°15′ W and near the grounding line may allow circulation between the two chambers beneath the Larsen C ice shelf.
3. MWDW, with a potential temperature above the surface pressure freezing point, impinges on the continental margin at depths of 500–800 m (Gordon, 1998; Absy and others, 2008). The troughs across the continental shelf thus provide access for this relatively warm water to the cavity beneath the ice shelf. Whether recent warming of WDW in the central part of the Weddell Sea (e.g. Robertson and others, 2002) has resulted in the transport of additional heat beneath the Larsen Ice Shelf and thus contributed to accelerated melting is unclear (Nicholls and others, 2004). Additional detailed oceanographic surveys along the front of the Larsen Ice Shelf are required to address this question.

ACKNOWLEDGEMENTS

We thank Michael Studinger, Nick Frearson, Stefan Elieff and Sean O'Rourke for their efforts during the 2009 IceBridge Antarctic field campaign. We also thank Bruce Huber for instructive discussions of Weddell Sea oceanography. Paul Holland provided us with his grid of ice-draft values for the Larsen C ice shelf. Hakim Abdi provided technical support. We also thank the anonymous referees and the scientific editor, Ted Scambos, for comments, criticisms and suggestions that greatly improved the manuscript. This work was supported by NASA grants NNX09AR49G, NNG10HP20C and NNX10AT69G. This is LDEO contribution No. 7526

REFERENCES

Absy JM, Schröder M, Muench R and Hellmer HH (2008) Early summer thermohaline characteristics and mixing in the western Weddell Sea. *Deep-Sea Res. II,* **55**(8–9), 1117–1131 (doi: 10.1016/j.dsr2.2007.12.023)

Bamber JL, Riva REM, Vermeersen BLA and LeBrocq AM (2009a) Reassessment of the potential sea-level rise from a collapse of the West Antarctic Ice Sheet. *Science,* **324**(5929), 901–903 (doi: 10.1126/science.1169335)

Bamber JL, Gomez-Dans JL and Griggs JA (2009b) *Antarctic 1 km Digital Elevation Model (DEM) from combined ERS-1 radar and ICESat laser satellite altimetry,* National Snow and Ice Data Center, Boulder, CO. Digital media: http://nsidc.org/data/docs/daac/nsidc0422_antarctic_1km_dem/index.html

Bamber JL, Gomez-Dans JL and Griggs JA (2009c) A new 1 km digital elevation model of the Antarctic derived from combined satellite radar and laser data – Part 1: data and methods. *Cryosphere,* **3**(1), 101–111 (doi: 10.5194/tc-3-101-2009)

Bell RE, Brozena JM, Haxby WF and LaBrecque JL (1990) Continental margins of the western Weddell Sea: insights from airborne gravity and Geosat-derived gravity. In *Contributions to Antarctic Research I.* American Geophysical Union, Washington, DC, 91–101 (Antaractic Research Series 50)

Carlson RL and Raskin GS (1984) Density of the ocean crust. *Nature,* **311**(5986), 555–558 (doi: 10.1038/311555a0)

Carmack E and Foster T (1977) Water masses and circulation in the Weddell Sea. In Dunbar MJ ed. *Polar oceans. Proceedings of the Polar Oceans Conference, May 1974, McGill University, Montreal, Canada.* Arctic Institute of North America, Calgary, Alb., 151–165

Cook AJ and Vaughan DG (2010) Overview of areal changes of the ice shelves on the Antarctic Peninsula over the past 50 years. *Cryosphere,* **4**(1), 77–98 (doi: 10.5194/tc-4-77-2010)

De Angelis H and Skvarca P (2003) Glacier surge after ice shelf collapse. *Science,* **299**(5612), 1560–1562

Del Valle RA, Elliot DH and Macdonald DIM (1992) Sedimentary basins on the east flank of the Antarctic Peninsula: proposed nomenclature. *Antarct. Sci.,* **4**(4), 477–478 (doi: 10.1017/S0954102092000695)

Del Valle RA, Lusky JC and Roura R (1998) Glacial trough under the Larsen Ice Shelf, Antarctic Peninsula. *Antarct. Sci.,* **10**(2), 173–174

Doake CSM, Corr HFJ, Rott H, Skvarca P and Young NW (1998) Breakup and conditions for stability of the northern Larsen Ice Shelf, Antarctica. *Nature,* **391**(6669), 778–780

Dowdeswell JA, Evans J, Ó Cofaigh C and Anderson JB (2006) Morphology and sedimentary processes on the continental slope off Pine Island Bay, Amundsen Sea, West Antarctica. *Geol. Soc. Am. Bull.,* **118**(5–6), 606–619 (doi: 10.1130/B25791.1)

Dupont TK and Alley RB (2005) Assessment of the importance of ice-shelf buttressing to ice-sheet flow. *Geophys. Res. Lett.,* **32**(4), L04503 (doi: 10.1029/2004GL022024)

https://doi.org/10.3189/2012JoG11J033 Published online by Cambridge University Press

Evans J, Pudsey CJ, Ó Cofaigh C, Morris P and Domack E (2005) Late Quaternary glacial history, flow dynamics and sedimentation along the eastern margin of the Antarctic Peninsula ice sheet. *Quat. Sci. Rev.,* **24**(5–6), 741–774 (doi: 10.1016/j.quascirev.2004.10.007)

Folland CK and 9 others (2001) Observed climate variability and change. In Houghton JT and 7 others eds. *Climate change 2001: the scientific basis. Contribution of Working Group I to the Third Assessment Report of the Intergovernmental Panel on Climate Change.* Cambridge University Press, Cambridge, 99–181

Glasser NF and Scambos TA (2008) A structural glaciological analysis of the 2002 Larsen B ice-shelf collapse. *J. Glaciol.,* **54**(184), 3–16 (doi: 10.3189/002214308784409017)

Glasser N and 7 others (2009) Surface structure and stability of the Larsen C ice shelf, Antarctic Peninsula. *J. Glaciol.,* **55**(191), 400–410 (doi: 10.3189/002214309788816597)

Gómez-Ortiz D and Agarwal BNP (2005) 3DINVER.M: a MATLAB program to invert the gravity anomaly over a 3D horizontal density interface by Parker Oldenburg's algorithm. *Comput. Geosci.,* **31**(4), 513–520 (doi: 10.1016/j.cageo.2004.11.004)

Gordon AL (1998) Western Weddell Sea thermohaline stratification. In Jacobs SS and Weiss RF eds. *Ocean, ice and atmosphere: interactions at the Antarctic continental margin.* American Geophysical Union, Washington, DC, 215–240 (Antarctic Research Series 75)

Gordon A and Huber BA (1990) Southern Ocean winter mixed layer. *J. Geophys. Res.,* **95**(C7), 11 655–11 672

Gordon AL and Huber BA (1995) Warm Weddell deep water west of Maud Rise. *J. Geophys. Res.,* **100**(C7), 13 747–13 753

Gordon AL and ISW Group (1993) Weddell Sea exploration from Ice Station. *Eos,* **74**(11), 121, 124–126

Griggs JA and Bamber JL (2009) Ice shelf thickness over Larsen C, Antarctica, derived from satellite altimetry. *Geophys. Res. Lett.,* **36**(19), L19501 (doi: 10.1029/2009GL039527)

Hathway B (2000) Continental rift to bark-arc basin: Jurassic-Cretaceous stratigraphical and structural evolution of the Larsen Basin, Antarctic Peninsula. *J. Geol. Soc. London,* **157**(2), 417–432

Hathway B, Macdonald DIM, Riding JB and Cantrill DJ (1998) Table Nunatak: a key outcrop of Upper Cretaceous shallow-marine strata in the southern Larsen Basin, Antarctic Peninsula. *Geol. Mag.,* **135**(4), 519–535

Hellmer HH, Jacobs SS and Jenkins A (1998) Oceanic erosion of a floating Antarctic glacier in the Amundsen Sea. In Jacobs SS and Weiss RF eds. *Ocean, ice and atmosphere: interactions at the Antarctic continental margin.* American Geophysical Union, Washington, DC, 83–100 (Antarctic Research Series 75)

Holland PR, Corr HFJ, Vaughan DG, Jenkins A and Skvarca P (2009) Marine ice in Larsen Ice Shelf. *Geophys. Res. Lett.,* **36**(11), L11604 (doi: 10.1029/2009GL038162)

Intergovernmental Panel on Climate Change (IPCC) (2007) Summary for policymakers. In Solomon S and 7 others eds. *Climate change 2007: the physical science basis. Contribution of Working Group I to the Fourth Assessment Report of the Intergovernmental Panel on Climate Change.* Cambridge University Press, Cambridge

Jacobs SS, Hellmer HH and Jenkins A (1996) Antarctic ice sheet melting in the southeast Pacific. *Geophys. Res. Lett.,* **23**(9), 957–960

Jansen D, Kulessa B, Sammonds PR, Luckman A, King EC and Glasser NF (2010) Present stability of the Larsen C ice shelf, Antarctic Peninsula. *J. Glaciol.,* **56**(198), 593–600 (doi: 10.3189/002214310793146223)

Jarvis EP and King EC (1993) The seismic wavefield recorded on an Antarctic ice shelf. *J. Seism. Explor.,* **2**(1), 69–86

Jarvis EP and King EC (1995) Seismic investigation of the Larsen Ice Shelf, Antarctica: in search of the Larsen Basin. *Antarct. Sci.,* **7**(2), 181–190

Jenkins A, Vaughan DG, Jacobs SS, Hellmer HH and Keys JR (1997) Glaciological and oceanographic evidence of high melt rates beneath Pine Island Glacier, West Antarctica. *J. Glaciol.,* **43**(143), 114–121

Jenkins A and 6 others (2010) Observations beneath Pine Island Glacier in West Antarctica and implications for its retreat. *Nature Geosci.,* **3**(7), 468–472 (doi: 10.1038/ngeo890)

Johnson MR and Smith AM (1997) Seabed topography under the southern and western Ronne Ice Shelf, derived from seismic surveys. *Antarct. Sci.,* **9**(2), 201–208

Jones PD and Moberg A (2003) Hemispheric and large-scale surface air temperature variations: an extensive revision and an update to 2001. *J. Climate,* **16**(2), 206–223 (doi: 10.1175/1520-0442(2003)016)

Ludwig WJ, Nafe JE and Drake CL (1971) Seismic refraction. In Maxwell AE ed. *The sea. Vol. 1, Part 4.* Wiley-Interscience, New York, 54–84

Lythe MB, Vaughan DG and BEDMAP consortium (2001) BEDMAP: a new ice thickness and subglacial topographic model of Antarctica. *J. Geophys. Res.,* **106**(B6), 11 335–11 351

MacAyeal DR, Scambos TA, Hulbe CL and Fahnestock MA (2003) Catastrophic ice-shelf break-up by an ice-shelf-fragment-capsize mechanism. *J. Glaciol.,* **49**(164), 22–36 (doi: 10.3189/172756503781830863)

Macdonald DIM and 6 others (1988) A preliminary assessment of the hydrocarbon potential of the Larsen Basin, Antarctica. *Mar. Petrol. Geol.,* **5**(1), 34–53 (doi: 10.1016/0264-8172(88)90038-4)

Maslanyi MP, Garrett SW, Renner RGB and Smith AM (1991) *GEOMAP: aeromagnetic anomaly map of West Antarctica (Weddell Sea sector), Sheet 2.* (BAS GEOMAP Series. Geophysical map and supplementary text.) British Antarctic Survey/Natural Environment Research Council, Cambridge

Mercer JH (1978) West Antarctic ice sheet and CO_2 greenhouse effect: a threat of disaster. *Nature,* **271**(5643), 321–325 (doi: 10.1038/271321a0)

Meredith MP, Locarnini RA, Van Scoy KA, Watson AJ, Heywood KJ and King BA (2000) On the sources of Weddell Gyre Antarctic bottom water. *J. Geophys. Res.,* **105**(C1), 1093–1104

Nicholls KW, Pudsey CJ and Morris P (2004) Summertime water masses off the northern Larsen C Ice Shelf. *Geophys. Res. Lett.,* **31**(9), L09309 (doi: 10.1029/2004GL019924)

Nielsen T and 8 others (2005) A comparison of the NW European glaciated margin with other glaciated margins. *Mar. Petrol. Geol.,* **22**(9–10), 1149–1183 (doi: 10.1016/j.marpetgeo.2004.12.007)

Oldenburg DW (1974) The inversion and interpretation of gravity anomalies. *Geophysics,* **39**(4), 526–536

Parker RL (1973) The rapid calculation of potential anomalies. *Geophys. J. Int.,* **31**(4), 447–455 (doi: 10.1111/j.1365-246X.1973.tb06513.x)

Pudsey CJ, Evans J, Domack EW, Morris P and Del Valle RA (2001) Bathymetry and acoustic facies beneath the former Larsen-A and Prince Gustav ice shelves, north-west Weddell Sea. *Antarct. Sci.,* **13**(3), 312–322 (doi: 10.1017/S095410200100044X)

Pudsey CJ, Murray JW, Appleby P and Evans J (2006) Ice shelf history from petrographic and foraminiferal evidence, Northeast Antarctic Peninsula. *Quat. Sci. Rev.,* **25**(17–18), 2357–2379 (doi: 10.1016/j.quascirev.2006.01.029)

Rack W and Rott H (2004) Pattern of retreat and disintegration of the Larsen B ice shelf, Antarctic Peninsula. *Ann. Glaciol.,* **39**, 505–510 (doi: 10.3189/172756404781814005)

Renner RGB, Sturgeon LJS and Garrett SW (1985) Reconnaissance gravity and aeromagnetic surveys of the Antarctic Peninsula. *BAS Sci. Rep.* 110

Rignot E, Casassa G, Gogineni P, Krabill W, Rivera A and Thomas R (2004) Accelerated ice discharge from the Antarctic Peninsula following the collapse of Larsen B ice shelf. *Geophys. Res. Lett.,* **31**(18), L18401 (doi: 10.1029/2004GL020697)

Rignot E and 6 others (2008) Recent Antarctic ice mass loss from radar interferometry and regional climate modelling. *Nature Geosci.,* **1**(2), 106–110 (doi: 10.1038/ngeo102)

Robertson R, Padman L and Levine MD (1995) Fine structure, microstructure, and vertical mixing processes in the upper ocean in the western Weddell Sea. *J. Geophys. Res.,* **100**(C9), 18 517–18 535

Robertson R, Visbeck M, Gordon AL and Fahrbach E (2002) Long-term temperature trends in the deep waters of the Weddell Sea. *Deep-Sea Res. II,* **49**(21), 4791–4806 (doi: 10.1016/S0967-0645(02)00159-5)

Rott H, Skvarca P and Nagler T (1996) Rapid collapse of northern Larsen Ice Shelf, Antarctica. *Science,* **271**(5250), 788–792

Rott H, Rack W, Skvarca P and De Angelis H (2002) Northern Larsen Ice Shelf, Antarctica: further retreat after collapse. *Ann. Glaciol.,* **34**, 277–282 (doi: 10.3189/172756402781817716)

Sander S, Argyle M, Elieff S, Ferguson S, Lavoie V and Sander L (2004) The AIRGrav airborne gravity system. In Lane R ed. *Airborne Gravity 2004: abstracts from the ASEG–PESA Airborne Gravity Workshop*. Geoscience Australia, Canberra, 49–53 (Geoscience Australia Record 2004/18) http://www.ga.gov.au/image_cache/GA16642.pdf

Scambos TA, Hulbe C, Fahnestock M and Bohlander J (2000) The link between climate warming and break-up of ice shelves in the Antarctic Peninsula. *J. Glaciol.,* **46**(154), 516–530 (doi: 10.3189/172756500781833043)

Scambos T, Hulbe C and Fahnestock M (2003) Climate-induced ice shelf disintegration in the Antarctic Peninsula. In Domack EW, Burnett A, Leventer A, Conley P, Kirby M and Bindschadler R eds. *Antarctic Peninsula climate variability: a historical and paleoenvironmental perspective*. American Geophysical Union, Washington, DC, 79–92 (Antarctic Research Series 79)

Scambos T and 7 others (2009) Ice shelf disintegration by plate bending and hydro-fracture: satellite observations and model results of the 2008 Wilkins ice shelf break-ups. *Earth Planet. Sci. Lett.,* **280**(1–4), 51–60 (doi: 10.1016/j.epsl.2008.12.027)

Shepard FP (1931) Glacial troughs of the continental shelves. *J. Geol.,* **39**(4), 345–360

Shepherd A, Wingham D, Payne T and Skvarca P (2003) Larsen ice shelf has progressively thinned. *Science,* **302**(5646), 856–859 (doi: 10.1126/science.1089768)

Shepherd A, Wingham D and Rignot E (2004) Warm ocean is eroding West Antarctic Ice Sheet. *Geophys. Res. Lett.,* **31**(23), L23404 (doi: 10.1029/2004GL021106)

Skvarca P, Rack W, Rott H and Donángelo T (1999) Climatic trend and the retreat and disintegration of ice shelves on the Antarctic Peninsula: an overview. *Polar Res.,* **18**(2), 151–157

Sloan BJ, Lauver LA and Anderson JB (1995) Seismic stratigraphy of the Larsen Basin, eastern Antarctic Basin Peninsula. In Cooper AK, Barker PF and Brancolini G eds. *Geology and seismic stratigraphy of the Antarctic margin*. American Geophysical Union, Washington, DC, 59–74 (Antarctic Research Series 68)

Smith RT and Anderson JB (2010) Ice-sheet evolution in James Ross Basin, Weddell Sea margin of the Antarctic Peninsula: the seismic stratigraphic record. *Geol. Soc. Am. Bull.,* **122**(5–6), 830–842 (doi: 10.1130/B26486.1)

Smith TM and Reynolds RW (2005) A global merged land–air–sea surface temperature reconstruction based on historical observations (1880–1997). *J. Climate,* **18**(12), 2021–2036 (doi: 10.1175/JCLI3362.1)

Smith WHF and Sandwell DT (1997) Global sea floor topography from satellite altimetry and ship depth soundings. *Science,* **277**(5334), 1956–1962

Studinger M, Bell R and Frearson N (2008) Comparison of AIRGrav and GT-1A airborne gravimeters for research applications. *Geophysics,* **73**(6), 151–161 (doi: 10.1190/1.2969664)

Turcotte DL and Schubert G (2002) *Geodynamics,* Cambridge University Press, Cambridge

Vaughan DG and Doake CSM (1996) Recent atmospheric warming and retreat of ice shelves on the Antarctic Peninsula. *Nature,* **379**(6563), 328–331

Vaughan DG and 9 others (1995) Subglacial and seabed topography, ice thickness and water column thickness in the vicinity of Filchner-Ronne-Shelf, Antarctica. *Polarforschung,* **64**(2), 75–88

Vaughan DG and 8 others (2003) Recent rapid regional climate warming on the Antarctic Peninsula. *Climatic Change,* **60**(3), 243–274

Vieli A, Payne AJ, Du Z and Shepherd A (2006) Numerical modelling and data assimilation of the Larsen B ice shelf, Antarctic Peninsula. *Philos. Trans. R. Soc. London, Ser. A,* **364**(1844), 1815–1839 (doi: 10.1098/rsta.2006.1800)

Walker DP, Brandon MA, Jenkins A, Allen JT, Dowdeswell JA and Evans J (2007) Oceanic heat transport onto the Amundsen Sea shelf through a submarine glacial trough. *Geophys. Res. Lett.,* **34**(2), L02602 (doi: 10.1029/2006GL028154)

Wellner JS, Lowe AL, Shipp SS and Anderson JB (2001) Distribution of glacial geomorphic features on the Antarctic continental shelf and correlation with substrate: implications for ice behavior. *J. Glaciol.,* **47**(158), 397–411 (doi: 10.3189/172756501781832043)

Weppernig R, Schlosser P, Khatiwala S and Fairbanks RG (1996) Isotope data from Ice Station Weddell: implications for deep water formation in the Weddell Sea. *J. Geophys. Res.,* **101**(C11), 25 723–25 739 (doi: 10.1029/96JC01895)

Wyer P and Watts AB (2006) Gravity anomalies and segmentation at the East Coast, USA continental margin. *Geophys. J. Int.,* **166**(3), 1015–1038 (doi: 10.1111/j.1365-246X.2006.03066.x)

MS received 27 February 2011 and accepted in revised form 15 January 2012